

# Journal of Engineering Sciences Faculty of Engineering Assiut University







journal homepage: http://jesaun.journals.ekb.eg

# Effects of Rotational Speed on Microstructure and Mechanical Properties of Friction Stir Spot-Welded AA6082-T6/AA1050 Dissimilar Lap Joints

Received 18 June 2025; Revised 4 September 2025; Accepted 5 September 2025

Abdelkarim Y. Mohamed<sup>1</sup> Elshafey Ahmed Gadallah<sup>2</sup> Mohamed M. E. Seleman<sup>3</sup> Medhat Elwan<sup>4</sup> Yousef G. Y. Elshaghoul<sup>5</sup> Hossam H. El-Fahhar<sup>6</sup>

#### **Keywords**

Friction stir spot welding, AA6082-T6, AA1050, Dissimilar lap joints, Mechanical properties, Microstructure, Rotational speed

Abstract: In this study, the macrostructure and mechanical characteristics of friction stir spot-welded (FSSWed) dissimilar lap joints between AA6082-T6 and AA1050 were investigated as a function of rotational speed. The FSSW procedure was carried out with a constant dwell time of 4 s and rotating speeds of 500, 700, and 900 rpm. The results showed that the heat input and maximum peak temperature increased by increasing the rotational speed, which improved material flow and wider bonding area between the upper and lower sheets. Microhardness measurements in the stir zone indicated an increase in higher value at lower rotational speeds, increasing from 86.9 HV at 900 rpm to 102.3 HV at 500 rpm, due to enhanced material flow, plastic deformation and re-precipitation of strengthening phases. Tensile-shear tests revealed a non-linear relationship between rotational speed and joint strength, with a maximum load of 4.58 kN at 500 rpm. Fracture analysis showed a shift from ductile fracture at lower speeds to a mix of ductile and smooth fracture features at higher speeds, indicating changes in the failure mechanism.

#### 1. Introduction

Lightweight materials, such as aluminum alloys, are crucial in the automotive and aerospace industries, where weight reduction without sacrificing structural integrity is critical [1–4]. The 6xxx series (Al-Mg-Si) alloys, such as AA6082-T6, are particularly popular due to their excellent strength, corrosion resistance, and weldability [5,6]. The 1xxx series alloys, such as AA1050, offer advantages such as good thermal/electrical conductivity and formability, albeit with reduced mechanical strength[7,8]. Combining these alloys in construction could maximize the strength of AA6082-T6 and the ductility or conductivity of AA1050, allowing

<sup>&</sup>lt;sup>1</sup> Mechanical Department (Production), Faculty of Technology and Education, Suez University, Suez, Egypt.

<sup>&</sup>lt;sup>2</sup> Mechanical Department (Production), Faculty of Technology and Education, Suez University, Suez, Egypt.

<sup>&</sup>lt;sup>3</sup> Metallurgical and Materials Engineering Department, Faculty of Petroleum and Mining Engineering, Suez University, Suez, Egypt.

<sup>&</sup>lt;sup>4</sup> Mechanical Department (Production), Faculty of Technology and Education, Suez University, Suez, Egypt.

<sup>&</sup>lt;sup>5</sup> Department of Mechanical Engineering, Faculty of Engineering, Suez University, Suez P.O. Box 43221, Egypt. Yousef.Gamal@eng.suezuni.edu.eg

<sup>&</sup>lt;sup>6</sup> Mechanical Department (Production), Faculty of Technology and Education, Suez University, Suez, Egypt

multifunctional engineering applications [9,10]. Combining dissimilar aluminum alloys presents challenges due to differences in thermal conductivity, melting temperature, and mechanical properties, complicating fusion-based spot-welding processes. These procedures often produce flaws like porosity and intermetallic formation, while mechanical fastening increases weight and expense[11]. Friction stir spot welding (FSSW), a solid-state joining technology that evolved from friction stir welding (FSW) [12–15], has emerged as a promising solution. FSSW prevents melting flaws, reduces heat distortion, and is appropriate for both similar and dissimilar materials[16,17]. The rotating speed during FSSW is crucial in determining process results, particularly when combining dissimilar aluminum alloys AA6082-T6 and AA1050. This parameter affects heat generation and material flow, causing microstructure changes in the weld zone [18]. These microstructural alterations influence the mechanical properties of the joint, such as its strength, durability, and overall performance. Understanding these effects is vital for improving welding procedures, ensuring high-quality lap joints, and advancing applications in industries that require lightweight and strong materials.

The procedure entails inserting a rotating tool into overlapping sheets, causing frictional heat to plasticize the material, followed by dwell time then tool retraction, resulting in a distinctive keyhole[19]. The resulting joint has four unique zones: a stir zone (SZ), a thermosmechanically affected zone (TMAZ), a heat-affected zone (HAZ), and a base material (BM)[20–23]. Despite its benefits, most FSSW research focuses on comparable aluminum alloys, particularly the AA6xxx series, at high rotational speeds (900-2500 rpm) [24,25]. Research is lacking on dissimilar combinations, particularly between AA1xxx and AA6xxx alloys, requiring investigations on joint behavior and parameter optimization. AA6082-T6, a heat-treatable alloy, is used for structural components, while AA1050, commercially pure aluminum, serves in applications needing formability and conductivity. Joining these alloys benefits businesses requiring hybrid constructions, such as heat exchangers with conductive fins (AA1050) and strong frames (AA6082). However, AA1050's higher thermal conductivity (~210 W/m·K) versus AA6082 (~170 W/m·K) may cause uneven heat distribution during FSSW, affecting material flow and joint integrity.

Based on a literature survey, no study has discussed the effect of varying rotational speeds and dwell times on the microstructure and mechanical performance of similar FSSW AA6082 lap joints. This study aims to address this gap by evaluating the effects of different rotational speeds (500, 700 and 900 rpm) with a constant dwell time of 4 s on the microstructure and mechanical behavior of the FSSW AA1050 and AA6082-T6 dissimilar sheets, as well as optimizing the parameters for dissimilar strong joints and advanced applications in lightweight structures.

# 2. Methodology

#### 2.1 Base Materials

This investigation utilized two different aluminum alloy sheets as the base materials. The upper sheet was AA6082-T6 aluminum alloy with a thickness of 2 mm, while the lower sheet was made of AA1050 aluminum alloy, with a thickness of 2 mm. These materials were

supplied in sheets of dimensions 1000 mm × 1000 mm. **Table 1** presents the chemical compositions of the AA6082-T6 and AA1050 base plates. **Table 2** summarizes the mechanical properties of the base materials. The chemical compositions (**Table 1**) and mechanical properties (**Table 2**) of AA6082-T6 and AA1050 were obtained from the supplier's certified material test reports (El-Nahas Company for Aluminum, Egypt and Fond Company, Milano, Italy).

**Table 1.** Chemical compositions of AA6082-T6 and AA1050 alloys.

Alloy	Element (wt.%)							
	Mg	Si	Fe	Mn	Cu	Ni	Al	
AA6082-T6	0.79	0.91	0.16	0.69	0.06	0.01	Bal	
AA1050	0.16	0.08	0.22	0.01	0.01	0.00	Bal	

**Table 2.** The mechanical properties of the base alloys, AA6082-T6 and AA1050.

Alloy	Property						
	Tensile strength (MPa)	Yield stress (MPa)	Hardness (HV)				
AA6082-T6	239	231	112.4				
AA1050	54	43	32.4				

#### 2.2 FSSW Process

The FSSW joints were produced using a friction stir welding/processing machine (EG-FSW-M1) was used to produce the FSSW joints [26–28]. For the welding procedure, both sheets were cut into specimens measuring 150 mm in length and 40 mm in width, The specimens were arranged in a lap-joint configuration with a 40 mm overlap between the upper and lower sheets. The FSSW process was conducted at various rotation speeds of 500, 700, and 900 rpm while maintaining a constant dwell time of 4 s. We sincerely thank the reviewer for raising this important point. The rotational speeds of 500, 700, and 900 rpm were selected based on preliminary experiments, which indicated that lower speeds (below 500 rpm) often result in insufficient heat input and incomplete material mixing, while higher speeds (above 900 rpm) may cause excessive thermal softening or tool wear in AA6082-T6. The other processing parameters were kept consistent throughout all experiments: a plunge depth of 3.2 mm, plunge rate of 0.1 mm/s, and tilt angle of 0°. The welding tool used in this study was fabricated from AISI H13 steel with a flat shoulder of 20 mm diameter and a cylindrical pin of 5 mm diameter and 2.8 mm length, as shown in Fig 1. This tool geometry was selected based on previous research demonstrating that cylindrical pin profiles produce axisymmetric temperature distributions and uniform heat transfer phenomena through the weld zone [29,30].

The complete FSSW process is depicted in Fig 2, which illustrates the process stages: (Fig 2a) clamping of the lap joint, (Fig 2b) positioning of the tool against the top plate of the lap joint, (Fig 2c) tool plunging and stirring action of the rotating tool, and (Fig 2d) tool retraction. Fig 2a also shows a representative real view of the applied tool geometry, and Fig 2d shows the top view of a completed spot-welded joint. The downward axial force (F) was measured in real-time using the machine's integrated load cell system. Surface temperature measurements were obtained using a calibrated infrared thermometer (Quicktemp 860-T3)

with  $\pm 1\%$  reading accuracy ( $\pm 2.5^{\circ}$ C), as illustrated in **Fig 2b**. The instrument was validated against embedded K-type thermocouples (OMEGA TJ36-CAXL-116U) at equivalent positions, showing <3% deviation across the measured range (200-400°C). Measurements were taken at a fixed 30 mm distance (45° angle) after verifying minimal emissivity variation (0.20 $\pm 0.02$  for both alloys at process temperatures). The analytical model for heat generation (Eqs. 1-5) is presented in Section 3.1 to directly correlate with measured thermal results.

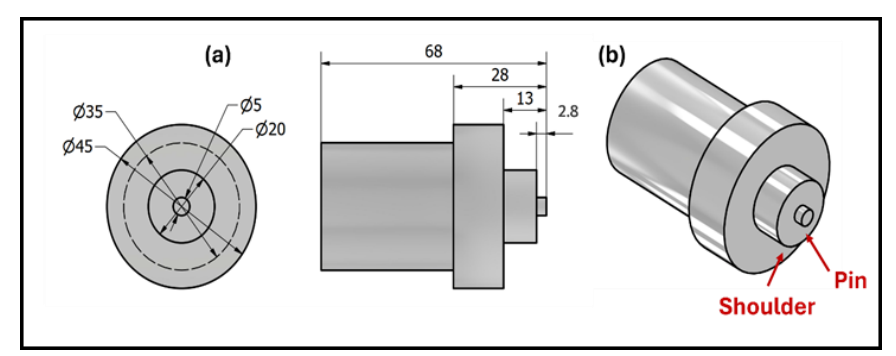


Fig 1. FSSW tool (a) dimension and (b) geometry (all dimensions in mm).

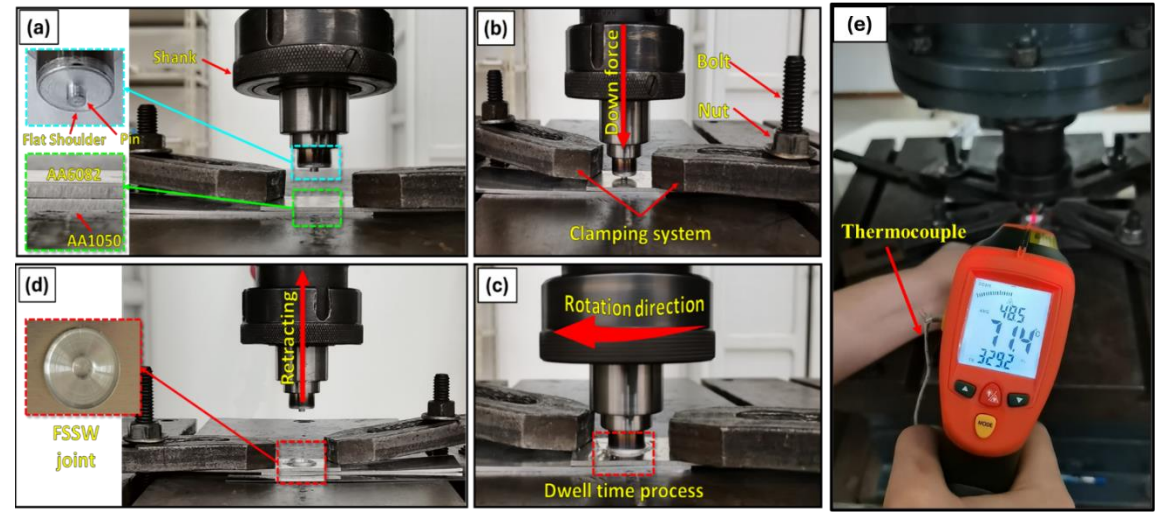
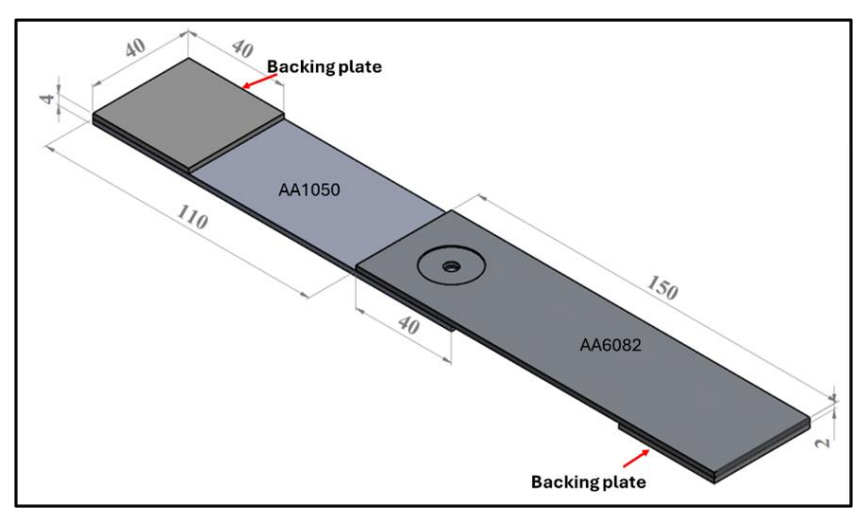


Fig 2. FSSW process stages for AA6082-T6/AA1050 dissimilar joints: (a) machine clamping system and tool geometry (b) applied downward force, (c) plunging and stirring process, (d) tool retraction and (e) recorded temperature via infrared thermometer.

#### 2.3 Microstructural and Mechanical Characterization

The welded lap joints were sectioned to examine their macrostructure and mechanical properties (hardness). Cross-sectional specimens were prepared by grinding with silicon carbide papers of increasing fineness up to 3000 grit, followed by polishing with alumina paste to achieve a surface finish of 0.05 µm. Chemical etching was performed using two different compositions of Keller's etchant to reveal the distinct microstructural features. The first etchant consisted of 25 ml of nitric acid (HNO<sub>3</sub>), 25 ml of hydrochloric acid (HCl), 25 ml of methanol (CH<sub>3</sub>OH), and one drop of hydrofluoric acid (HF). The second etchant was composed of 2.5 ml HNO<sub>3</sub>, 1.5 ml HCl, 95 ml distilled water, and 1 ml HF. Hardness testing was performed across the weld cross-sections using a Vickers hardness tester (model HWDV-75) with an applied load of 3 N and a dwell time of 15 s. The average of eight measurements around the stir zone was recorded to explore the average hardness of the

dissimilar FSSWed lap joints. Tensile-shear testing was performed on a 30-ton universal testing machine (Type-WDW-300D) at room temperature with a constant loading rate of 0.1 mm/s. Tensile-shear specimens were prepared in accordance with ASTM E8M-04. For each rotational speed, three replicate joints were tested to calculate average tensile-shear loads and standard deviations, ensuring statistical reliability. **Fig 3** presents schematic diagrams of the tensile-shear test specimens for the FSSW joint. "Backing sheets (2 mm thick AA1050 and 1 mm thick AA6082) were used to prevent bending and ensure axial alignment during tensile-shear testing, as illustrated in **Figs 3,4**. Following the Tensile-shear test, Fracture surface specimens were cleaned ultrasonically in acetone for 10 minutes to remove debris. SEM imaging was performed using a Quanta FEG 250 microscope at an accelerating voltage of 15 kV, working distance of 10 mm, and spot size of 4.0. Secondary electron (SE) mode was employed at magnifications of 500×-3000× to capture ductile dimple morphology and cleavage features to evaluate the failure mechanisms and correlate them with the microstructural features and mechanical performance of the joints.



**Fig 3.** Schematic of FSSW AA6082/1050 tensile-shear test sample, including the backing plate to ensure uniform load distribution. All dimensions are in mm

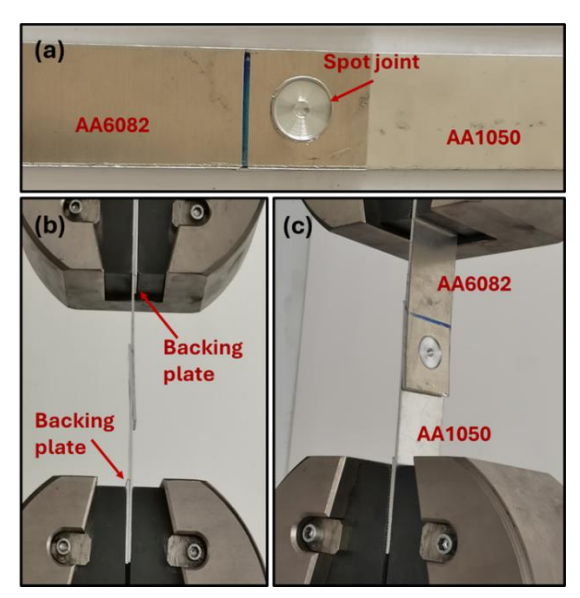


**Fig 4.** Tensile-shear test setup: (a) dissimilar FSSWed AA6082-T6/AA1050 lap joint and (b, c) two different views of the tensile-shear testing arrangement with backing plate.

# 3. Results

# 3.1. Heat Generation and Temperature Measurements

The heat generated during FSSW is a critical parameter that significantly influences joint quality and mechanical properties. The thermal energy produced during the FSSW of AA6082-T6/AA1050 dissimilar lap joints is primarily governed by a complex interplay of processing parameters. Analysis of the thermal phenomena reveals that the heat input is significantly influenced by tool geometry, rotational speed, dwell time, and the applied downward force [31–33]. The thermomechanical process of converting rotational mechanical energy into heat can be quantified through analytical modeling. Based on previous works [34,35], the instantaneous frictional power (Q) generated during FSSW can be expressed by Eq. 1:

$$Q = \frac{13}{12} \times \mu \times \frac{F}{K_A} \times \omega \times Rp \qquad \to Eq. 1$$

where Q has units of watts (J/s). The total thermal energy input is obtained by integrating this power over the dwell time.

μis friction coefficient between the steel tool and aluminum alloy (approximately 0.4 for this material combination [36–38].

- F is the downward force (N).
- $K_A$  is the ratio of the contact area of the shoulder profile to the cross-sectional tool area.
- $\omega$  is the angular speed in rad/s.
- Rp is a pin radius.

The friction coefficient ( $\mu = 0.4$ ) was selected based on extensive characterization of steel-aluminum pairs in FSSW literature[36,37]. This value represents typical sticking-sliding conditions at elevated temperatures (250-400°C.

The angular speed in rad/s can be calculated using Eq. 2:

$$\omega = \frac{2 \times \pi}{60} \times Rn \longrightarrow Eq. 2$$

• Rn is a member of the revolution per second.

The value of Rn can be calculated using Eq. 3:

$$Rn = \frac{R(rpm)}{60} \times t(s) \rightarrow Eq.3$$

- R is the applied rotation speed in rpm.
- t is the dwell time in s.

For the specific tool geometry employed in this study, the  $K_A$  value was calculated according to Eq.4:

$$KA = \frac{Rs^2 - Rp^2}{Rs^2} = 0.9375$$
  $\to Eq. 4$ 

- Rs is the shoulder radius in mm.
- Rp is pin radius in mm.

Based on Eqs. 1-4, Total thermal energy input (kJ) for the AA6082-T6/AA1050 dissimilar lap joints during the FSSW process at the applied process parameters were calculated according to Eq. 5:

$$Q = 0.120948 \times F \times R \qquad \rightarrow Eq.5$$

Table 3 presents the calculated thermal energy inputs and measured peak temperatures during the FSSW of AA6082-T6/AA1050 dissimilar lap joints at different rotational speeds while maintaining a constant dwell time of 4 s. The results demonstrated a clear correlation between the rotational speed and both the thermal energy input and peak temperature. As the rotational speed increased from 500 to 900 rpm, the calculated thermal energy input increased proportionally from 4.6 to 7.65 kJ. This 66% increase in thermal energy reflects the direct relationship between the rotational speed and heat generation during the FSSW process. The thermal energy input calculations were based on Eqs. 1-4 provide valuable insights into process optimization. Eq. 5 was established for this specific tool geometry and material combination, offers a practical means of predicting the thermal energy input for various processing parameters.

Similarly, the measured peak temperatures exhibited a consistent upward trend that corresponded to increasing rotational speeds. The peak temperature increased from 256 °C at 500 rpm to 303 °C at 700 rpm and further increased to 354°C at 900 rpm, as shown in **Table 3**. This represents a temperature increase of approximately 37% over the tested speed range. The observed temperature increase was consistent with the calculated increase in the thermal energy input, confirming the strong correlation between these parameters. The relationship between the applied rotational speed and thermal phenomena can be understood through the fundamental mechanics of the FSW process. Higher rotational speeds increase the frictional interaction between the tool and workpiece material, thereby generating more heat at the interface. This is mathematically represented by Eq.1, where the angular velocity ( $\omega$ ) directly influences the thermal energy (Q) generated during the process. The experimental results confirmed this theoretical relationship, with a nearly linear increase in both the calculated thermal energy and maximum measured peak temperature with increasing rotational speed.

**Table 3**. Thermal energy input and peak temperature during FSSW process at different rotation speeds.

	Re	otation speed (r	pm)
	500	700	900
Total thermal energy input (kJ)	4.6	6.32	7.65
Peak temperature (°C)	256	303	354

Fig. 5 illustrates the relationship between the calculated thermal energy input and peak temperature during the FSSW of AA6082-T6/AA1050 dissimilar lap joints. Fig. 5 shows a strong positive linear correlation between these two parameters, with a coefficient of determination (R<sup>2</sup>) of 0.9866. This exceptionally high R<sup>2</sup> value confirms that approximately 98.66% of the variation in maximum peak temperature can be directly attributed to changes in the thermal energy input, demonstrating the predictive capability of the thermal energy model developed in this study. While the strong linear correlation ( $R^2 = 0.9866$ ) suggests a consistent relationship between calculated heat input and maximum measured peak temperatures, several limitations apply: (1) the model assumes constant friction coefficient and perfect thermal contact, (2) IR measurements have  $\pm 8^{\circ}$ C uncertainty near joint edges (see Section 2.2), and (3) the three-speed dataset provides limited coverage of possible parameter space. The linear regression equation derived from the experimental data (y = 30.881 x + 114.18) provides a practical tool for predicting peak temperatures based on the calculated thermal energy inputs. This relationship indicates that for every 1 kJ increase in thermal energy input, the peak temperature increases by approximately 30.9°C within the operational range studied. This substantial positive correlation validates the theoretical framework established using Eqs. 1-4, confirming that the simplified model of eq.5 effectively captures the heat generation mechanics in the FSSW process for this specific material combination and tool geometry. These findings align with previous research by Ahmed et al. [36–38]. and Ataya et al. [35], they reported similar linear correlations between processing parameters and thermal responses in friction stir welding processes, though with different slopes and intercepts due to variations in material properties and tool geometries. The present study extends these observations to the specific case of dissimilar AA6082-T6/AA1050 lap joints, providing valuable reference data for the industrial applications of this welding configuration.

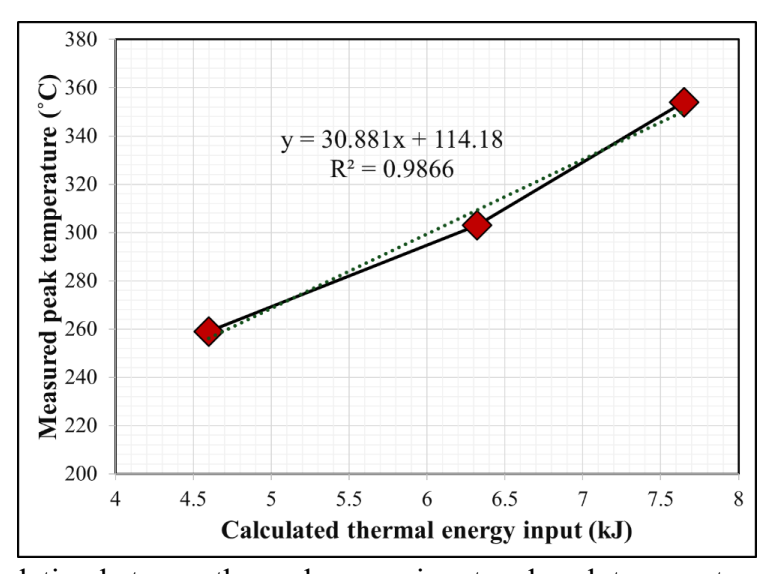
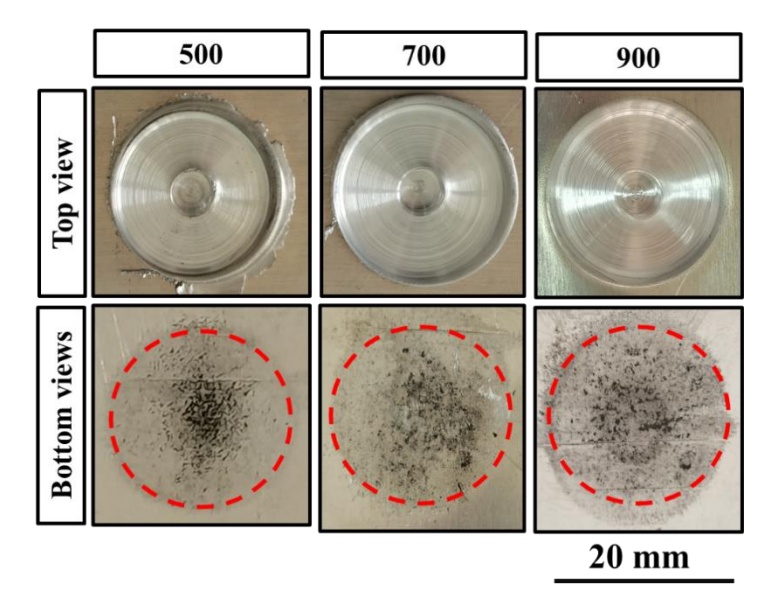


Fig. 5. Linear correlation between thermal energy input and peak temperature for the lap joints.

# 3.2. Visual Analysis of FSSW Joints

**Fig. 6** presents a comparative visual analysis of the FSSW joints produced using dissimilar AA6082-T6/AA1050 alloys. The specimens were processed at a constant dwell time of 4 s while varying the rotational speeds of 500, 700, and 900 rpm, revealing distinct morphological patterns on both the top and bottom surfaces. The top-surface morphologies in Fig. 6 show

well-defined circular shoulder impressions at all rotational speeds, indicating consistent tool engagement and effective surface consolidation. The shoulder marks appear smooth and uniform, with minimal tearing or surface defects, suggesting stable material plasticization under the applied process parameters. The slight increase in the sharpness of the shoulder periphery at 900 rpm can be attributed to the higher heat input softening the material, allowing cleaner shoulder imprinting. Furthermore, the material extrusion along the rim of the shoulder imprint is minimal at 500 rpm, reflecting controlled flow due to lower heat and plasticity. At 700 rpm, extrusion becomes slightly more evident, indicating increased plasticization and outward flow. At 900 rpm, the extrusion ring is more pronounced, forming a fine peripheral flash this is consistent with the elevated heat input energy (7.65 kJ) promoting excess material displacement beyond the shoulder zone. In the bottom views of Fig. 6, the progressive change in thermal footprint coloration—from light at 500 rpm to dark and well-defined at 900 rpm provides a clear visual indication of increased heat generation and conduction through the joint thickness as the rotational speed rises. The darker shades and sharper boundaries at higher speeds reflect both elevated peak temperatures and longer exposure of the lower sheet to the softened, thermomechanically agitated material above. This phenomenon suggests that, at higher rotational speeds, the enhanced frictional heat not only facilitates more intense material mixing but also allows a greater proportion of thermal energy to be transferred radially and axially, enlarging the thermally affected rim zone. The enlargement of this rim zone is consistent with the calculated heat inputs (Table 3), where the 66% increase in energy from 500 to 900 rpm promotes a more pronounced thermal gradient extending outward from the pin contact area. The evidence from thermal footprints underscores the interdependence between rotational speed, heat conduction pathways, and the resulting plasticized flow behavior. In particular, the intensified thermal impact at 900 rpm may facilitate easier outward displacement of material, leading to the observed peripheral flash. The varying thermal footprints provide visual evidence of the relationship between the process parameters and energy input during FSSW.



**Fig. 6.** Top and bottom views of FSSWed dissimilar AA6082/AA1050 lap joints welded at a dwell time of 4 s.

## 3.3. Cross-Sectional Macrostructure and Flow Behavior

This section examines the interplay between rotational speed, macrostructural evolution, and material flow patterns in the FSSW joints. Cross-sectional analysis reveals how process parameters govern keyhole formation, stir zone geometry, and defect distribution. Fig. 7 shows the macrostructural cross-sectional views of the FSSW lap joints produced at various rotational speeds. The specimens were processed with a constant dwell time of 4 s while varying the rotational speeds to 500, 700, and 900 rpm. In all specimens, effective bonding occurred at the interface between the overlapped sheets, demonstrating the successful application of plastic deformation and material flow induced by the rotating tool pin. The SZ exhibited characteristic geometrical features, with keyhole formation evident in the central region, which is a typical artifact of the FSSW process. The upper sheet material underwent significant deformation beneath the tool shoulder, whereas the material flow patterns around the pin area exhibited varying characteristics depending on the rotational speed. The macrostructural cross-sections in Fig. 7 reveal clear variations in the geometry of the SZ and the morphology of the keyhole as a function of rotational speed. At 500 rpm, the SZ exhibits relatively wide, continuous boundaries between the upper and lower sheets, reflecting material flow under moderate heat input. The keyhole opening is uniform and sharply defined, indicating minimal distortion during tool retraction. At 700 rpm, the SZ widens further in the upper region due to enhanced plasticization and more vigorous stirring but also displays slight asymmetry in its lateral boundaries, likely caused by increased turbulence in material flow. The keyhole at this speed appears marginally larger at the top and tapers more abruptly toward the root, indicating that higher heat input softened the surrounding material. At 900 rpm, the SZ becomes comparatively narrower despite higher heat input. The keyhole at this speed shows less uniformity, with subtle wall irregularities and partial closure at the lower end, possibly due to viscous backflow of the plasticized material during the final stages of tool retraction. This partial closure could also be associated with the rapid solidification of the highly heated lower sheet surface, as evidenced by the pronounced thermal footprint in Fig. 6. It can be concluded that the SZ and keyhole morphologies reflect the competing effects of rotational speed on material flow: while low rotation speeds of 500 ad 700 rpm encourage lateral stirring and broader SZ formation, higher rotation speeds of 900 rpm may over-soften the material, altering the flow path and producing narrower, less symmetrical profiles.

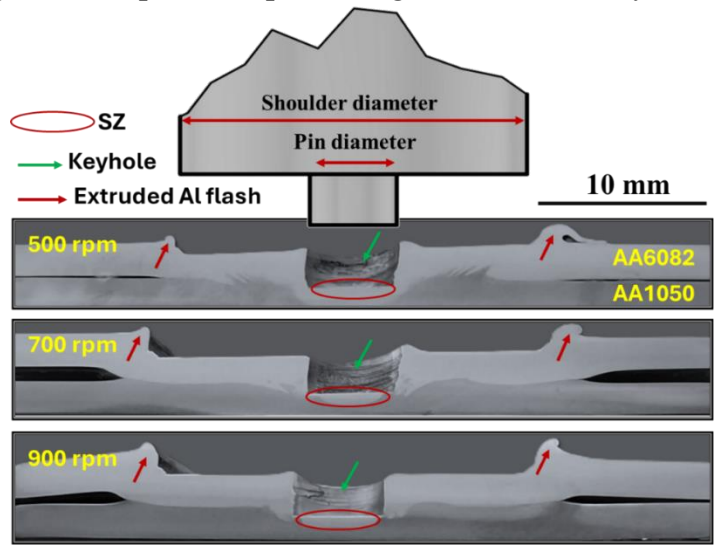
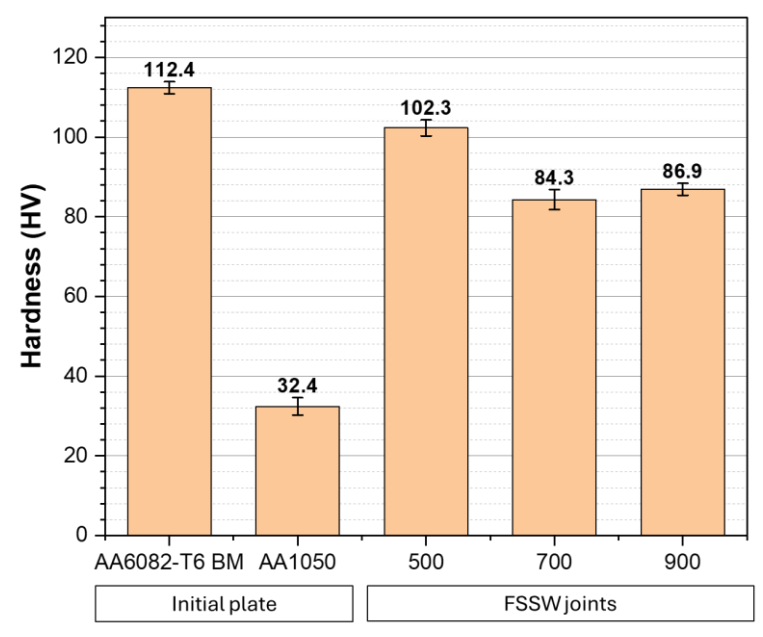


Fig. 7. Cross-sectional macrostructure of AA6082/AA1050 lap joints produced at varying rotation speeds with fixed dwell time.

#### 3.4. Hardness

**Fig. 8** presents microhardness results for the SZ of AA6082-T6/AA1050 dissimilar FSSW lap joints at different rotational speeds with a constant dwell time of 4 s. The base materials showed substantially different hardness values, with AA6082-T6 measuring 112.4 HV and AA1050 measuring 32.4 HV. This difference of 3.5 times is attributed to the chemical composition and temper of AA6082-T6, which contains strengthening precipitates, primarily Mg<sub>2</sub>Si, that enhance its mechanical properties compared to AA1050 [21].

The hardness values of the SZ in FSSWed joints were between those of both materials, indicating effective mixing during FSSW. At 500 rpm, the average hardness in the SZ was 102.3 HV, decreasing to 84.3 HV at 700 rpm, then slightly increasing to 86.9 HV at 900 rpm. This nonlinear trend shows a hardness reduction of 15.4% between 500 rpm and 900 rpm conditions. The intermediate hardness values in the SZ can be attributed to concurrent metallurgical phenomena. The material in the SZ represented a mixture of the two dissimilar alloys, resulting in composition between AA6082-T6 and AA1050. However, the SZ hardness values are closer to AA6082-T6 than AA1050, suggesting the stronger alloy's properties dominate the joint characteristics.



**Fig. 8.** Average hardness values at the SZ of FSSWed AA6082/AA1050 dissimilar lap joints welded at a dwell time of 4 s.

This dominance can be attributed to the position of AA6082-T6 as the upper sheet, where it experienced more significant deformation due to the tool shoulder and pin [39]. The observed hardness reduction with increasing rotational speed can be directly correlated with the thermal energy input and peak temperatures listed in **Table 3** as follows: at higher rotational speeds, the increased heat generation of 7.65 kJ at 900 rpm compared to 4.6 kJ at 500 rpm enhanced the material plasticity but also caused greater thermal softening. This thermal effect is particularly significant for the AA6082-T6 alloy, where the T6 temper involves artificially aged precipitates that contribute to its strength [5,40]. The higher peak temperatures of 354°C at 900 rpm compared to 256°C at 500 rpm likely caused partial dissolution or coarsening of these strengthening precipitates, leading to the observed hardness reduction [40]. The slight recovery in hardness at 900 rpm compared to 700 rpm suggests the presence of competing

mechanisms at the highest rotational speed. This finding is consistent with those of other studies on similar aluminum alloys. For instance, Patel et al. [37] investigated the dissimilar FSSW of AA5052-H32 and AA6082-T6 and they reported that the hardness in the SZ increased with tool rotation speed due to enhanced mechanical intermixing at higher rpm. In the same context, Arif et al. [41] applied the FSW for AA5083 and AA6061-T6 dissimilar joints, increasing rotational speed from 900 to 2280 rpm led to grain coarsening and more homogeneous mixing in the SZ, increasing hardness and tensile strength. The relationship between hardness and rotational speed also aligns with the macrostructural features observed in **Fig. 7**, where higher rotational speeds produced more pronounced material flow patterns and wider affected zones. Despite the enhanced material flow and mixing at higher rotational speeds, the thermal softening effect appears to be the dominant factor influencing the hardness of these dissimilar joints.

## 3.5. Tensile-Shear results

**Fig. 9** shows the tensile-shear load capacities of AA6082-T6/AA1050 dissimilar FSSWed lap joints processed at different rotational speeds of 500, 700, and 900 rpm while maintaining a constant dwell time of 4 s. The tensile-shear load results revealed a distinct nonlinear relationship between rotational speed and joint mechanical performance, with the highest tensile-shear load of 4.58 kN observed at 500 rpm, followed by a significant decrease to 3.95 kN at 700 rpm and a slight recovery to 4.06 kN at 900 rpm, as shown in **Fig. 9**.

The highest tensile-shear performance at the lowest rotational speed of 500 rpm can be attributed to several factors. First, the lower heat input at 500 rpm (4.6 kJ, as shown in Table 3) produced a more favorable microstructural balance in SZ. At this processing condition, the peak temperature reached only 259°C, which is significantly below the solutioning temperature of AA6082-T6, approximately 530°C [42,43]. This moderate temperature increase was sufficient to enable adequate plastic deformation and material flow for joint formation while minimizing detrimental microstructural transformations. Lower thermal exposure helped preserve some of the strengthening precipitates in the AA6082-T6 alloy, which would otherwise dissolve at higher temperatures, contributing to superior mechanical performance.

The tensile-shear load decreased by approximately 13.76% when the rotational speed increased from 500 to 700 rpm, and then a slight recovery in tensile-shear performance was observed at 900 rpm, with 4.06 kN compared to 700 rpm, representing a 2.8% increase, suggesting a competing balance between adverse thermal effects and beneficial mechanical mixing. Although the highest thermal energy input of 7.65 kJ and peak temperature of approximately 354°C were recorded at 900 rpm, the enhanced material flow and mixing at this speed may have improved the mechanical interlocking between the dissimilar alloys, partially offsetting the negative thermal effects. This is supported by the macrostructural observations in **Fig. 7**, which show more pronounced material extrusion and wider affected zones at higher rotational speeds.

A direct correlation can be observed between the mechanical properties of hardness and tensile-shear load results. At 500 rpm, both the hardness of 102.3 HV and tensile-shear load of 4.58 kN reached their maximum values, followed by significant decreases at 700 rpm with 84.3 HV and 3.95 kN, and then modest recoveries at 900 rpm with 86.9 HV and 4.06 kN,

respectively. This correlation can be attributed to the competing metallurgical phenomena that occur during FSSW at different rotational speeds. At 500 rpm, the moderate heat input of 4.6 kJ provided sufficient material plasticity for effective bonding while preserving much of the strengthening precipitates in the AA6082-T6 alloy, resulting in both higher hardness and superior tensile-shear performance. The increased heat input of 6.32 kJ at 700 rpm caused significant thermal softening through precipitate dissolution or coarsening, thereby reducing both the hardness and joint strength. At 900 rpm, despite the further increase in thermal softening from the highest heat input of 7.65 kJ, the enhanced material flow and mixing produced better mechanical interlocking and potentially finer reprecipitated structures during cooling, explaining the slight recovery in both properties.

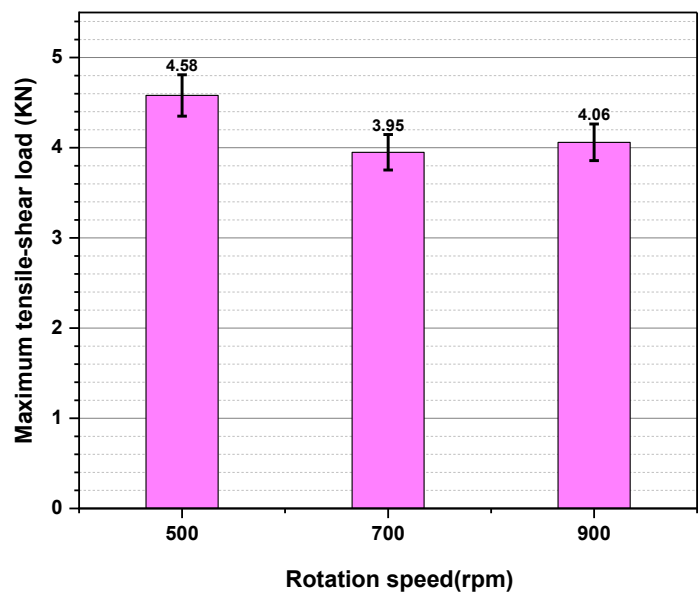


**Fig. 9.** Tensile-shear load of FSSW AA6082/AA1050 lap joints at 500, 700, and 900 rpm. Error bars represent standard deviation (SD) from n = 3 replicates per condition. Average values are marked with horizontal lines.

**Fig. 10** presents SEM images of the fracture surfaces of the base materials (**Figures 10a and 10b**) and dissimilar AA6082-T6/AA1050 FSSWed lap joints produced at rotational speeds of 500 rpm (**Fig. 10c**), 700 rpm (**Fig. 10d**), and 900 rpm (**Fig. 10e**). The fracture surface of the AA6082-T6 base material, shown in Figure 10(a), exhibited a mixed mode of fracture with predominantly dimpled features characteristic of ductile fracture, interspersed with relatively smooth regions. The dimple structures varied in size and depth, indicating the nucleation, growth, and coalescence of microvoids during plastic deformation.

The presence of flat regions suggests partial brittle fracture behavior, consistent with the higher strength and moderate ductility of the T6 tempered condition of this alloy. In contrast, the AA1050 base material, as shown in **Fig 10b**, exhibited a highly dimpled surface with deeper and more uniformly distributed dimples, indicating a predominantly ductile fracture mechanism. The extensive plastic deformation evident in these dimples aligns with the lower strength but higher ductility of this commercially pure aluminum alloy, which lacks the strengthening precipitates present in AA6082-T6.

The fracture surfaces of the FSSWed joints exhibited complex morphologies that reflected the combined influence of material mixing, thermal history, and loading conditions. The specimen welded at 500 rpm (Fig. 10c) exhibited a fracture surface with well-defined dimple structures and limited smooth regions, suggesting effective material bonding and ductile failure mechanisms. As the rotational speed increased to 700 rpm (Fig. 10d), the fracture surface exhibited more elongated dimples and larger smooth areas, indicating a shift in the failure mechanism. The reduced density of dimples and their more irregular distribution suggest less effective material mixing or potential microstructural defects, which aligns with the significant decrease in the tensile-shear load capacity to 3.95 kN under this processing condition. The observed morphology indicated a combination of ductile tearing and quasicleavage fracture mechanisms. At the highest rotational speed of 900 rpm (Fig. 10e), the fracture surface shows a partial recovery of dimple features compared to the 700 rpm specimen, but with more variable dimple sizes and depths. In addition, some smooth regions and less pronounced dimple structures were observed compared to the 500 rpm specimen. The combination of fine dimples and smooth regions suggests improved material flow and mixing compared with the 700 rpm condition, which corresponds with the slight recovery in the tensile-shear performance to 4.06 kN.

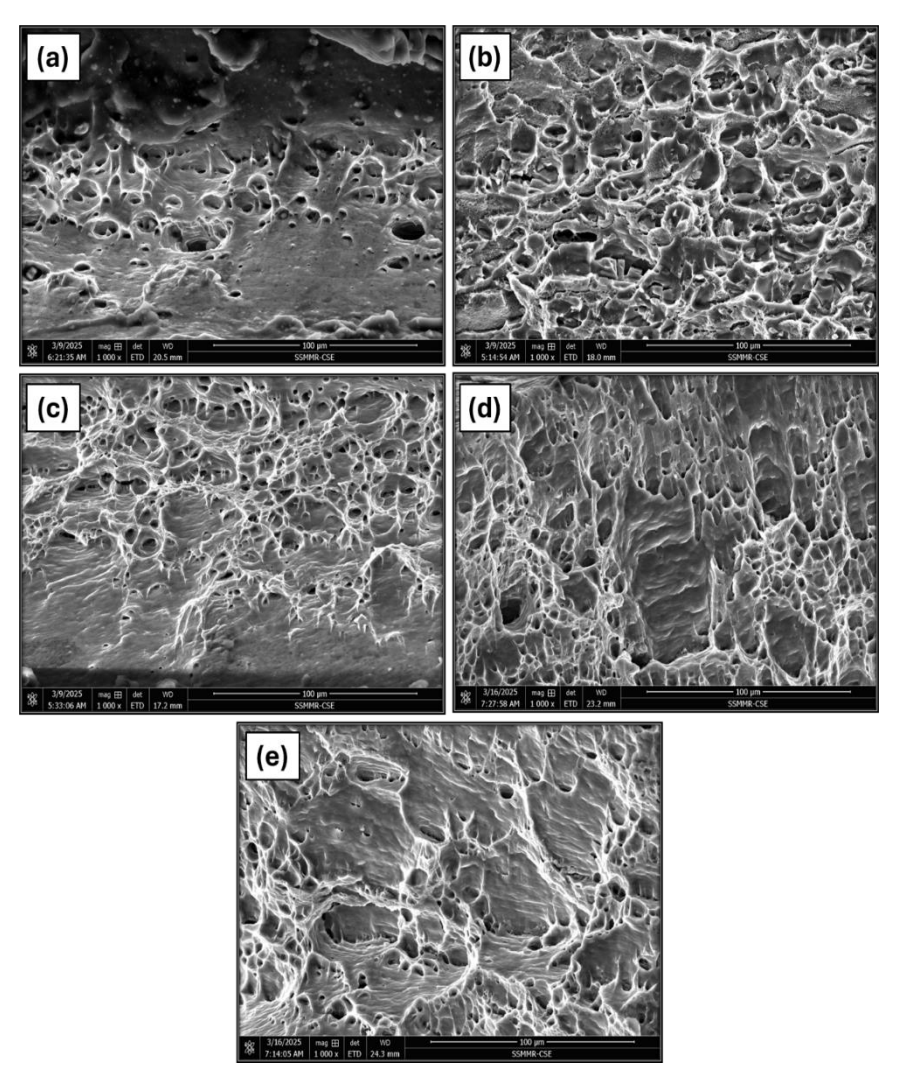


Fig. 10. Fracture surfaces of (a) AA1050, (b) AA6082-T6 BM and the FSSWed lap joints produced at rotation speeds of (c) 500, (d) 700, and (e) 900 rpm.

#### 4. Conclusions

This study investigated the effect of rotational speed on the microstructure, mechanical properties, and fracture behaviour of friction stir spot-welded AA6082-T6/AA1050 dissimilar lap joints. The study revealed several significant findings:

- The thermal energy generation exhibited a direct linear relationship with rotational speed, increasing by 66% from 4.6 to 7.65 kJ when the rotational speed increased from 500 to 900 rpm, with a corresponding 37% rise in peak temperature from 256°C to 354°C.
- Microstructural analysis demonstrated effective material flow and bonding at all speeds but with distinct patterns: higher rotational speeds produced broader affected zones and more pronounced material extrusion, indicating enhanced material mixing and greater thermal exposure. This trade-off was reflected in the microhardness measurements, where the values in the stir zone decreased by 17.6%, from 102.3 HV at 500 rpm to 84.3 HV at 700 rpm, followed by a modest 3.1% recovery to 86.9 HV at 900 rpm.
- The joint strength exhibited a nonlinear relationship with the rotational speed, with a maximum tensile-shear load of 4.58 kN achieved at 500 rpm, which decreased by 13.76% to 3.95 kN at 700 rpm, followed by a 2.8% recovery to 4.06 kN at 900 rpm.
- Fracture surface analysis revealed a transition from predominantly ductile dimple structures at 500 rpm to a mixture of dimples and smooth regions at higher speeds, providing microstructural evidence for the observed changes in mechanical properties.
- For AA6082-T6/AA1050 dissimilar FSSW joints, a rotational speed of 500 rpm provided an optimal balance between thermal input and mechanical mixing.

#### References

- 1. Kumar, S.; Jambhale, S.; Maurya, M.; Kumar, S.; Pandey, S. Evaluation of Shear Force and Fractography of Friction Stir Spot Welded Joints of AA 6082-T6 Alloy. *Journal of Engineering Research (Kuwait)* **2022**, *10*, 124–144, doi:10.36909/jer.10265.
- 2. Ahmed, M.M.Z.; El-Sayed Seleman, M.M.; Ahmed, E.; Reyad, H.A.; Alsaleh, N.A.; Albaijan, I. A Novel Friction Stir Deposition Technique to Refill Keyhole of Friction Stir Spot Welded AA6082-T6 Dissimilar Joints of Different Sheet Thicknesses. *Materials* **2022**, *15*, doi:10.3390/ma15196799.
- 3. Essa, A.R.S.; Aboud, A.R.K.; Ahmed, M.M.Z.; El-Nikhaily, A.E.; Easa, A.S.; Habba, M.I.A. Friction Stir Welding of Aluminum Alloy 6082-T6 Using Eccentric Shoulder Tools to Eliminate the Need for Tool Tilting. *Sci Rep* **2025**, *15*, doi:10.1038/s41598-025-91065-1.
- 4. El-Fahhar, H.H.; Gadallah, E.A.; Habba, M.I.A.; Seleman, M.M.E.-S.; Ahmed, M.M.Z.; Mohamed, A.Y.; Fouad, R.A. Effect of Post-Weld Heat-Treatment and Solid-State Thermomechanical Treatment on the Properties of the AA6082 MIG Welded Joints. *Sci Rep* **2024**, *14*, doi:10.1038/s41598-024-53795-6.
- 5. Ahmed, M.M.Z.; Seleman, M.M.E.S.; Ahmed, E.; Reyad, H.A.; Touileb, K.; Albaijan, I. Friction Stir Spot Welding of Different Thickness Sheets of Aluminum Alloy AA6082-T6. *Materials* **2022**, *15*, doi:10.3390/ma15092971.
- 6. Alzahrani, B.; Ahmed, M.M.Z.; Habba, M.I.A.; Fouad, R.A.; Elshaghoul, Y.G.Y.; Gadallah, E.A. TIG Welding of EN AW-6082 Al Alloy: A Comparative Analysis of Filler Rods on Microstructural and Mechanical Performance. *Journal of Manufacturing and Materials Processing* **2025**, *9*, doi:10.3390/jmmp9010021.

- 7. I. A. Habba, M.; Kh. Younis, M.; Sadoun, A.M.; Fathy, A.; Barakat, W.S. On the Microstructural and Mechanical Responses of Dual-Matrix Al-Ni/SiC Composites Manufactured Using Accumulative Roll Bonding. *Alexandria Engineering Journal* **2023**, *78*, 1–14, doi: 10.1016/j.aej.2023.07.030.
- 8. Elwan, M.; Fathy, A.; Wagih, A.; Essa, A.R.S.; Abu-Oqail, A.; El-Nikhaily, A.E. Fabrication and Investigation on the Properties of Ilmenite (FeTiO3)-Based Al Composite by Accumulative Roll Bonding. *J Compos Mater* **2020**, *54*, 1259–1271.
- 9. Ahmed, M.M.Z.; El-Sayed Seleman, M.M.; Eid, R.G.; Zawrah, M.F. Production of AA1050/Silica Fume Composite by Bobbin Tool-Friction Stir Processing: Microstructure, Composition and Mechanical Properties. *CIRP J Manuf Sci Technol* **2022**, *38*, 801–812, doi: 10.1016/J.CIRPJ.2022.07.002.
- 10. Barakat, W.S.; Kh. Younis, M.; Sadoun, A.M.; Fathy, A.; Habba, M.I.A. Optimization of the Accumulative Roll Bonding Process Parameters and SiC Content for Optimum Enhancement in Mechanical Properties of Al-Ni-SiC Composites. *Alexandria Engineering Journal* **2023**, *76*, 131–151, doi: 10.1016/j.aej.2023.06.027.
- 11. Aydin, H.; Tuncel, O.; Umur, Y.; Tutar, M.; Bayram, A. *Effect of Welding Parameters on Microstructure and Mechanical Properties of Aluminum Alloy AA6082-T6 Friction Stir Spot Welds*; 2017; Vol. 24;.
- 12. Elshaghoul, Y.G.Y.; El-Sayed Seleman, M.M.; Bakkar, A.; Elnekhaily, S.A.; Albaijan, I.; Ahmed, M.M.Z.; Abdel-Samad, A.; Reda, R. Additive Friction Stir Deposition of AA7075-T6 Alloy: Impact of Process Parameters on the Microstructures and Properties of the Continuously Deposited Multilayered Parts. *Applied Sciences (Switzerland)* **2023**, *13*, doi:10.3390/app131810255.
- 13. Habba, M.I.A.; Ahmed, M.M.Z. Friction Stir Welding of Dissimilar Aluminum and Copper Alloys: A Review of Strategies for Enhancing Joint Quality. *Journal of Advanced Joining Processes* **2025**, *11*, doi: 10.1016/j.jajp.2025.100293.
- 14. Habba, M.I.A.; Ahmed, M.M.Z. Friction Stir Welding-Based Technologies: A Comprehensive Review from the Sustainable Manufacturing Perspectives. *Journal of Materials Research and Technology* **2025**, *38*, 1–29, doi: 10.1016/J.JMRT.2025.07.184.
- 15. Sadoun, A.M.; Wagih, A.; Fathy, A.; Essa, A.R.S. Effect of Tool Pin Side Area Ratio on Temperature Distribution in Friction Stir Welding. *Results Phys* **2019**, *15*, doi: 10.1016/j.rinp.2019.102814.
- 16. Ahmed, M.M.Z.; El-Sayed Seleman, M.M.; Albaijan, I.; Abd El-Aty, A. Microstructure, Texture, and Mechanical Properties of Friction Stir Spot-Welded AA5052-H32: Influence of Tool Rotation Rate. *Materials* **2023**, *16*, doi:10.3390/ma16093423.
- 17. Rabea, M.F.; Fouad, R.A.; El-Sayed Seleman, M.M.; Ahmed, E. Effect of Dwell Time on Mechanical and Metallurgical Behavior of Dissimilar FSSWed Cu-S355 JR Lap Joints. *The International Journal of Advanced Manufacturing Technology* **2025**, *138*, 873–894, doi:10.1007/s00170-025-15565-0.
- 18. Ikuta, A.; Yin, Y.H.; North, T.H. Influence of Tool Thread on Mechanical Properties of Dissimilar Al Alloy Friction Stir Spot Welds. *Science and Technology of Welding and Joining* **2012**, *17*, 622–629, doi:10.1179/1362171812Y.0000000053.
- 19. Abbass, M.K.; Hussein, S.K.; Khudhair, A.A. Optimization of Mechanical Properties of Friction Stir Spot Welded Joints for Dissimilar Aluminum Alloys (AA2024-T3 and AA 5754-H114). *Arab J Sci Eng* **2016**, *41*, 4563–4572, doi:10.1007/s13369-016-2172-9.
- 20. Khosa, S.U.; Weinberger, T.; Enzinger, N. Thermo-Mechanical Investigations during Friction Stir Spot Welding (FSSW) of AA6082-T6. *Welding in the World* **2010**, *54*, R134–R146, doi:10.1007/BF03263499.

- 21. Ouis, A.; Habba, M.I.A.; Ahmed, M.M.Z.; Barakat, W.S. Tribological and Corrosion Behavior of Al2O3 Interlayer Reinforced Friction Stir Welded AA6082-T6 Joints. *Sci Rep* **2025**, *15*, 22437, doi:10.1038/s41598-025-03977-7.
- 22. Sadoun, A.M.; Meselhy, A.F.; Deabs, A.W. Improved Strength and Ductility of Friction Stir Tailor-Welded Blanks of Base Metal AA2024 Reinforced with Interlayer Strip of AA7075. *Results Phys* **2020**, *16*, doi: 10.1016/j.rinp.2019.102911.
- 23. Habba, M.I.A.; Ahmed, M.M.Z.; Fouad, R.A.; Barakat, W.S. Friction Stir Welding of AA6082-T6 Assisted with a Novel Encapsulated Alumina Interlayer: Surface Morphology, Tribology, and Topographic Analysis. *The International Journal of Advanced Manufacturing Technology* **2025**, *139*, 2823–2845, doi:10.1007/s00170-025-16063-z.
- 24. Mabuwa, S.; Msomi, V. The Effect of Friction Stir Processing on the Friction Stir Welded AA1050-H14 and AA6082-T6 Joints. *Mater Today Proc* **2020**, *26*, 193–199.
- 25. Zhang, Z.K.; Yu, Y.; Zhang, J.F.; Wang, X.J. Corrosion Behavior of Keyhole-Free Friction Stir Spot Welded Joints of Dissimilar 6082 Aluminum Alloy and DP600 Galvanized Steel in 3.5% NaCl Solution. *Metals (Basel)* **2017**, 7, doi:10.3390/met7090338.
- 26. Ahmed, M.M.Z.; Hajlaoui, K.; Seleman, M.M.E.-S.; Elkady, M.F.; Ataya, S.; Latief, F.H.; Habba, M.I.A. Microstructure and Mechanical Properties of Friction Stir Welded 2205 Duplex Stainless Steel Butt Joints. *Materials* **2021**, *14*, doi:10.3390/ma14216640.
- 27. Habba, M.I.A.; Alsaleh, N.A.; Badran, T.E.; El-Sayed Seleman, M.M.; Ataya, S.; El-Nikhaily, A.E.; Abdul-Latif, A.; Ahmed, M.M.Z. Comparative Study of FSW, MIG, and TIG Welding of AA5083-H111 Based on the Evaluation of Welded Joints and Economic Aspect. *Materials* **2023**, *16*, doi:10.3390/ma16145124.
- 28. Ahmed, M.S.I.; Ahmed, M.M.Z.; Abd El-Aziz, H.M.; Habba, M.I.A.; Ismael, A.F.; El-Sayed Seleman, M.M.; Abd El-Aty, A.; Alamry, A.; Alzahrani, B.; Touileb, K.; et al. Cladding of Carbon Steel with Stainless Steel Using Friction Stir Welding: Effect of Process Parameters on Microstructure and Mechanical Properties. *Crystals (Basel)* **2023**, *13*, doi:10.3390/cryst13111559.
- 29. Essa, A.R.S.; Ahmed, M.M.Z.; Mohamed, A.-K.Y.A.; El-Nikhaily, A.E. An Analytical Model of Heat Generation for Eccentric Cylindrical Pin in Friction Stir Welding. *Journal of Materials Research and Technology* **2016**, *5*, 234 240, doi: 10.1016/j.jmrt.2015.11.009.
- 30. Gadakh, V.S.; Adepu, K. Heat Generation Model for Taper Cylindrical Pin Profile in FSW. *Journal of Materials Research and Technology* **2013**, 2, 370–375, doi: 10.1016/j.jmrt.2013.10.003.
- 31. Wiedenhoft, A.G.; Amorim, H.J. de; Rosendo, T. de S.; Tier, M.A.D.; Reguly, A. Effect of Heat Input on the Mechanical Behaviour of Al-Cu FSW Lap Joints. *Materials Research* **2018**, *21*, e20170983.
- 32. Ahmed, M.M.Z.; Ataya, S.; El-Sayed Seleman, M.M.; Mahdy, A.M.A.; Alsaleh, N.A.; Ahmed, E. Heat Input and Mechanical Properties Investigation of Friction Stir Welded Aa5083/Aa5754 and Aa5083/Aa7020. *Metals (Basel)* **2020**, *11*, 68.
- 33. Essa, A.R.S.; Eldersy, R.I.A.; Ahmed, M.M.Z.; Abd El-Aty, A.; Alamry, A.; Alzahrani, B.; El-Nikhaily, A.E.; Habba, M.I.A. Modeling and Experimental Investigation of the Impact of the Hemispherical Tool on Heat Generation and Tensile Properties of Dissimilar Friction Stir Welded AA5083 and AA7075 Al Alloys. *Materials* **2024**, *17*, doi:10.3390/ma17020433.
- 34. Atak, A.; Sik, A.; Ozdemir, V. Thermo-Mechanical Modeling of Friction Stir Spot Welding and Numerical Solution with the Finite Element Method. *International Journal of Engineering and Applied Sciences* **2018**, *5*, 257275.

- 35. Ataya, S.; Ahmed, M.M.Z.; El-Sayed Seleman, M.M.; Hajlaoui, K.; Latief, F.H.; Soliman, A.M.; Elshaghoul, Y.G.Y.; Habba, M.I.A. Effective Range of FSSW Parameters for High Load-Carrying Capacity of Dissimilar Steel A283M-C/Brass CuZn40 Joints. *Materials* **2022**, *15*, 1394.
- 36. Tamadon, A.; Pons, D.J.; Sued, K.; Clucas, D. Thermomechanical Grain Refinement in AA6082-T6 Thin Plates under Bobbin Friction Stir Welding. *Metals (Basel)* **2018**, *8*, 375.
- 37. Patel, V. V.; Sejani, D.J.; Patel, N.J.; Vora, J.J.; Gadhvi, B.J.; Padodara, N.R.; Vamja, C.D. Effect of Tool Rotation Speed on Friction Stir Spot Welded AA5052-H32 and AA6082-T6 Dissimilar Aluminum Alloys. *Metallography, Microstructure, and Analysis* **2016**, *5*, 142–148, doi:10.1007/S13632-016-0264-2.
- 38. Ahmed, M.M.Z.; Habba, M.I.A.; Jouini, N.; Alzahrani, B.; El-Sayed Seleman, M.M.; El-Nikhaily, A. Bobbin Tool Friction Stir Welding of Aluminum Using Different Tool Pin Geometries: Mathematical Models for the Heat Generation. *Metals (Basel)* **2021**, *11*, 1–19, doi:10.3390/met11030438.
- 39. Ahmed, M.M.Z.; El-Sayed Seleman, M.M.; Sobih, A.M.E.S.; Bakkar, A.; Albaijan, I.; Touileb, K.; Abd El-Aty, A. Friction Stir-Spot Welding of AA5052-H32 Alloy Sheets: Effects of Dwell Time on Mechanical Properties and Microstructural Evolution. *Materials* **2023**, *16*, doi:10.3390/ma16072818.
- 40. Koumoulos, E.P.; Charitidis, C.A.; Daniolos, N.M.; Pantelis, D.I. Nanomechanical Properties of Friction Stir Welded AA6082-T6 Aluminum Alloy. *Materials Science and Engineering: B* **2011**, *176*, 1585–1589, doi: 10.1016/J.MSEB.2011.01.015.
- 41. Arif, W.; Ilman, M.N.; Iswanto, P.T.; Kusmono; Akhyar The Effect of Tool Rotation Speed on Hardness, Tensile Strength, and Microstructure of Dissimilar Friction Stir Welding of Dissimilar AA5083 and AA6061-T6 Alloys. *Key Eng Mater* **2021**, *892*, 159–168, doi: 10.4028/WWW.SCIENTIFIC.NET/KEM.892.159.
- 42. Tamadon, A.; Pons, D.J.; Clucas, D.; Sued, K. Internal Material Flow Layers in AA6082-T6 Butt-Joints during Bobbin Friction Stir Welding. *Metals (Basel)* **2019**, *9*, doi:10.3390/MET9101059.
- 43. Moreira, P.M.G.P.; Santos, T.; Tavares, S.M.O.; Richter-Trummer, V.; Vilaça, P.; de Castro, P.M.S.T. Mechanical and Metallurgical Characterization of Friction Stir Welding Joints of AA6061-T6 with AA6082-T6. *Mater Des* **2009**, *30*, 180–187, doi: 10.1016/J.MATDES.2008.04.042.